ISSN 2093-8551
Vol. 1, No. 1, 2010, 31-38
DOI:10.5229/JECST.2010.1.1.031

Journal of Electrochemical Science and Technology

Fine Structure Effect of PdCo electrocatalyst for Oxygen Reduction Reaction Activity: Based on X-ray Absorption Spectroscopy Studies with Synchrotron Beam

Dae-Suk Kim, Tae-Jun Kim, Jun-Hyuk Kim, E. F. Abo Zeid and Yong-Tae Kim†
School of Mechanical Engineering, Pusan National University, Jangjeon-dong, Geumjeong-gu, Busan 609-735, Korea

ABSTRACT :

In this study, we have demonstrated the fine structure effect of PdCo electrocatalyst on oxygen reduction reaction activity with different alloy composition and heat-treatment time. In order to identify the intrinsic factors for the electrocatalytic activity, various X-ray analyses were used, including inductively coupled plasma-atomic emission spectrometer, transmission electron microscopy, X-ray diffractometer, and X-ray Absorption Spectroscopy technique. In particular, extended X-ray absorption fine structure was employed to extract the structural parameters required for understanding the atomic distribution and alloying extent, and to identify the corresponding simulated structures by using FEFF8 code and IFEFFIT software. The electrocatalytic activity of PdCo alloy nanoparticles for the oxygen reduction reaction was evaluated by using rotating disk electrode technique and correlated to the change in structural parameters. We have found that Pd-rich surface was formed on the Co core with increasing heating time over 5 hours. Such core shell structure of PdCo/C showed that a superior oxygen reduction reaction activity than pure Pd/C or alloy phase of PdCo/C electrocatalysts, because the adsorption energy of adsorbates was apparently reduced by lowering the d-band center of the Pd skin due to a combination of the compressive strain effect and ligand effect.

Keywords : Electrocatalysts, Oxygen reduction reaction, PdCo alloy, XANES, EXAFS.

Received August 30, 2010 : Accepted September 8, 2010

1. Introduction

Platinum and its alloys supported on carbon are commonly used as electrocatalysts for the oxygen reduction reaction (ORR) in fuel cells, however their high cost poses serious challenges for commercialization.[1-3] Recently, alloying of Pd of which the cost is only one-fifth of Pt with other elements has been found to show high catalytic activity for ORR.[4-9] Among them, the PdCo alloys are particularly interesting as they exhibit high catalytic activity for ORR and also good tolerance to methanol.[4,10] Many researchers reported that the particle size, dispersion, and compositional homogeneity of the alloy clusters on the carbon support are important factors to obtain good catalytic activity.[11-13]

In the theoretical calculations and experimental data, Pd-based alloys undergo phase segregations by annealing at high temperatures, with the noble metal Pd migrating to the surface forming a pure Pd overlayer on the bulk alloys.[14,15] The electronic structures of the metal overlayers can be significantly altered upon bonding with the substrate metal, and thus their catalytic properties can be changed.[16,17] Therefore, the understanding relationship between the catalytic activity and the fine structure is the key factor to design desirable electrocatalysts. However, little is known about the effect of PdCo alloy structure on the catalytic activity.

In the present paper, PdCo/C bimetallic catalysts with different atomic ratios were prepared by a borohydride reduction method and then heat-treated for different heat-

†Corresponding author. Tel.: +82-51-510-1012
E-mail address: yongtae@pusan.ac.kr

treatment time to understand relationship between the ORR activity and the fine structure effect of PdCo catalysts. Cyclic voltammetry (CV) and ORR with rotating disk electrode (RDE) were carried out to evaluate the electrocatalytic activity. The effect of heat-treatment time on PdCo electrocatalysts was characterized by Inductively coupled plasma-atomic emission spectrometer (ICP-AES), X-ray diffraction (XRD), and Transmission electron microscopy (TEM). In particular, the X-ray absorption near edge structure (XANES) region providing critical information about the oxidation state of d-electron density and the extended X-ray absorption fine structure (EXAFS) region providing details about a local structure in the vicinity of the absorbing atom[18-21] were used to discuss recently introduced Nørskov's d-band model,[16,17,22,23] with revealing the corresponding simulated structure using a program IFEFFIT.[24-27]

2. Experimental

2.1. Catalyst synthesis

Carbon-supported 20 wt%Pd_xCo_{100-X} (x = 100, 70, and 30) electrocatalysts were prepared by means of the borohydride reduction method. First, carbon (Vulcan XC-72R) was finely dispersed in DI water with 70 kHz frequency sonication for 10 min. After sonication, $Pd(NH_3)_4Cl_2 \cdot H_2O$(Alfa Aesar) and $CoCl_2 \cdot 6H_2O$ (Daejung chemicals), equivalent to 20% weight ratio of PdCo to carbon, were dissolved in the above solution with stirring for 30 min. Subsequently, $NaBH_4$ (Kanto chemical) dissolved in DI water was rapidly dropped into the precursor solution with vigorous stirring for 12 h, thus the PdCo precursor was simultaneously reduced and supported on the carbon support. In the borohydride reduction process, no surfactant/stabilizer was employed. The precipitate was filtered and washed several times with DI water and ethanol, and dried overnight in a vacuum oven at 70°C. After drying, we obtained Pd_xCo_{100-X} (x = 100, 70 and 30) supported on the carbon support electrocatalysts. PdCo/C electrocatalysts were then heat-treated at 300°C in a flowing 100% H_2 gas for 1 h and 5 h. Pd_{100}/C electrocatalyst was not heated. To take $Pd_{70}Co_{30}$/C as an example, obtained $Pd_{70}Co_{30}$/C heated at 300°C for 1 h and 5 h were referred to in the present paper as $Pd_{70}Co_{30}$/C (1 h), and $Pd_{70}Co_{30}$/C (5 h), respectively. The $Pd_{30}Co_{70}$/C samples were also referred to as the same way.

2.2. Catalyst characterization

The weight percentage of Pd_xCo_{100-X} in the catalysts investigated by inductively coupled plasma-atomic emission spectrometer (ICP-AES) analysis in Korea basic science institute (KBSI) Busan Center after preprocessing Pd_xCo_{100-x}/C samples with dispersing them in the mixture of hydrochloric acid and nitric acid, mixed in a volum ratio of 3 : 1, and then heated at 300°C for 3 h.

The morphology of electrocatalyst samples was investigated using transmission electron microscopy (TEM, JEOL JEM-2011) in KBSI Busan Center. Specimens for TEM observation were prepared by placing a drop of the particle-dispersed ethanol solution onto a copper grid; then, the TEM was operated at an accelerating voltage of 200 keV. All of the images were recorded with a charge-coupled device (CCD) camera.

XRD measurements of Pd_xCo_{100-X} catalysts were carried out on a Philips Pan analytical X-ray diffractometer in KBSI Daegu Center using Cu K_α radiation λ = 0.15406 nm. The XRD spectra were obtained using high resolution in the step-scanning mode with a counting time of 5 s per 0.08°. Scans were recorded in the 2θ range of 10-90°.

X-ray absorption near edge structure (XANES) and extended X-ray absorption fine structure (EXAFS) data for the energies of Pd (24350 eV) K absorption edges were obtained in fluorescent mode with the synchrotron radiation of X-ray Absorption Fine Structure Spectroscopy II (7C1), Pohang Light Source (PLS), at room temperature. X-rays were monochromated with double crystal monochromator and detected by ion chambers, which were continuously purged with a gas mixture of He and N_2 to prevent any air contamination during the experiments. Gas-filled ion chambers were used in series to measure the intensities of the incident beam (I_0), the beam transmitted by the sample (I_t), the fluorescent bream by the sample (I_f), and the bream subsequently transmitted by the reference foil (I_r). The third ion chamber was used in conjunction with the reference sample, which was a Pd foil for the Pd K-edge measurements. Every experiment on PdCo/C nanoparticles was conducted on a homemade cell fabricated with an aluminum holder for XAS powder experiments. All of the spectra were recorded at room temperature. The spectra were processed by using a program IFEFFIT[24-27] (version 1.2.11c, IFEFFIT Copyright 2008, Matthew Newville, University of Chicago, http://cars9.uchicago.edu/ifeefit/) with background subtraction (AUTOBK)[28] and normailization. The phase shift and back scattering amplitude were calculated theoretically using FEFF 8.4 code.[29] Fourier transform for EXAFS spectra was performed in the range of ca. 1-16 $Å^{-1}$ in k-space and 1-3 Å in R-space with the

first-shell single scattering paths and k^3 weighted. From these analyses, structural parameters such as coordination numbers (N), bond distance (R), and Debye-Waller factor ($\Delta\sigma_j^2$) have been calculated.

2.3. Electrochemical measurements

All electrochemical measurements were performed in a three-electrode electrochemical cell on a potentiostat (Biologic VSP) at room temperature. A thin-layer rotating disk electrode (5 mm in diameter) was used as a working electrode, which was polished with Al_2O_3 slurries and washed in DI water with sonication before the experiments. Well dispersed 5 mg of PdCo/C powder in 2 ml of DI water using an ultrasonicator was deposited onto a glassy carbon electrode by dropping 20 μl with a micropipette for 2 times, resulting in PdCo loading in 20 $\mu g/cm^2_{electrode}$. Uniform thin PdCo/C films were prepared by evaporating the water at room temperature. Nafion solution (0.025 wt.%, 20 μL) was dropped onto a suspension-dried rotating disk electrode and dried in a vacuum oven at 70°C for 30 min. A platinum wire and a silver chloride electrode (Ag/AgCl sat 3.5 M KCl) were used as a counter and a reference electrode. Cyclic voltammetry (CV) measurements were performed in O_2-free 0.1 M $HClO_4$electrolyte obtained by bubbling high-purity N_2 gas for 30 min. The electrodes were cycled in the potential range between –0.195 and 1.005 V versus Ag/AgCl at a scan rate of 20 mV/s after electrochemical cleaning with a quick scan (scan rate: 200 mV/s) for 50 cycles. After CV measurements, oxygen reduction reaction (ORR) was subsequently performed in the same potential range in oxygen-saturated 0.1 M $HClO_4$ at rotating speeds of 100, 400, 900, 1600, and 2500 rpm with a scan rate of 5 mV/s. All of the current densities were normalized to the geometric area of the rotating disk electrode.

3. Results and Discussion

The exact alloy composition of carbon-supported of Pd_xCo_{100-X} electrocatalysts prepared by using the borohydride reduction method were evaluated with ICP-AES analysis. Table 1 shows Pd_xCo_{100-X} weight percentage in the catalysts determined by ICP-AES analysis. Pd and PdCo showed that nearly 16 wt% of electrocatalysts.

The particle size and distribution of Pd/C and PdCo/C electrocatalysts were characterized by TEM observation. TEM images of (a) Pd_{100}/C, (b) $Pd_{30}Co_{70}$/C(1 h), (c) $Pd_{30}Co_{70}$/C(5 h), (d) $Pd_{70}Co_{30}$/C(1 h), (e) $Pd_{70}Co_{30}$/C(5 h) are shown in Fig. 1. Pd nanoparticles were highly dispersed on the carbon vulcan supports with the diameter 5-7 nm in Fig. 1(a). However, due to the heating at 300°C with flowing H_2 gas, the diameter of PdCo nanoparticles was increased by agglomerating themselves with the diameter around 10 nm in Fig. 1(b-e). In addition, the size of PdCo nanoparticles was slightly more grown with the increased heat-treatment time from 1h to 5 h.

Table 1. Pd_xCo_{100-X} weight percentage in the catalysts determined by ICP-AES analysis

Sample	Pd (ppm)	Co (ppm)	PdCo wt%
Pd_{100}/C	15.1	N.D.	15.1
$Pd_{30}Co_{70}$/C (1 h)	5.4	12.4	17.8
$Pd_{30}Co_{70}$/C (5 h)	5.4	12.3	17.7
$Pd_{70}Co_{30}$/C (1h)	10.6	4.1	14.7
$Pd_{70}Co_{30}$/C (5 h)	11.4	4.4	15.8

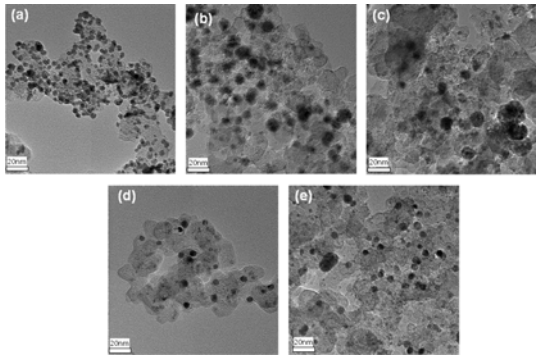

Fig. 1. TEM images of electrocatalysts (a) Pd_{100}/C, (b) $Pd_{30}Co_{70}$/C (1 h), (c) $Pd_{30}Co_{70}$/C(5 h), (d) $Pd_{70}Co_{30}$/C(1 h) and (e) $Pd_{70}Co_{30}$/C (5 h).

X-ray diffraction patterns of Pd_{100}/C and a series of PdCo/C electrocatalysts are presented in Fig. 2. The left side peak located at $2\theta = 25^o$ corresponds to the Carbon Vulcan support. The other principal peaks exhibited fcc crystalline Pd(JCPDS Card 00-005-0681);[30] (111), (200), (220), and (311) located at 40, 47, 68, 82, respectively. The Pd (111) peak position was shifted to the high angle on alloying with Co, implying that the lattice contraction was occurred due to smaller atomic radius of Co. It is interesting to note that the peak position was however shifted to the low angle with increasing heat treatment time from 1h to 5 h for both alloy samples. Such fact indicates that the structure of electrocatalysts was changed from alloy phase to unalloyed Pd and Co during heat treatment. There is an inconsistency in particle size from TEM image and XRD FWHM: In the

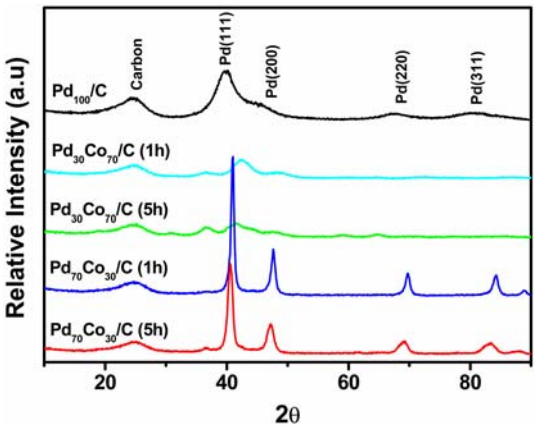

Fig. 2. X-ray diffraction patterns of Pd_{100}/C and Pd_xCo_{100-X} electrocatalysts.

case of $Pd_{30}Co_{70}/C$, even though the particle size was roughly 10 nm from the TEM images which is similar size with $Pd_{70}Co_{30}/C$, the FWHM of XRD is too large. This discordance can be elucidated with the amorphous metallic structure of $Pd_{30}Co_{70}/C$, so that the diffraction interaction is weak, albeit they seem to be 10 nm-sized particles in the bright field images of TEM.

X-ray absorption near edge structure (XANES) spectra was investigated to identify the electronic properties in terms of the oxidation state, the fractional d-electron density, and electronic environment of the absorbing atom of PdCo/C electrocatalysts. Fig. 3(a) shows XANES data of the Pd K-edge for Pd_{100}/C and a series of PdCo/C peaks.The white line of Pd K-edge energy for PdCo/C was decreased as alloying with Co implying a decreased occupancy in the 4d band compared to pure Pd/C. Several recent literatures[4,31-34] reported that to enhance the catalytic activity of a Pd-based catalyst, the ε_d (d-band center) of Pd should be shifted to a lower-energy position, meaning that the catalytic activity of the metals is significantly affected by the shift of the d-band center.[16,17,22,23] Based on the XANES results, the ε_d of Pd is expected to downshift owing to the smaller vacancy of the 4d band in the PdCo/C with heat-treatments as suggested by previous literature,[4] thereby leading to the higher ORR activity.

The extended X-ray absorption fine structure (EXAFS) region, which can provide details about the number, type, and distance of the backscattering atom surrounding the central absorbing atom, allows investigations on the short-range ordering and geometric information, and provides the electronic state of characteristic of electrocatalyst. Fig. 3(c)

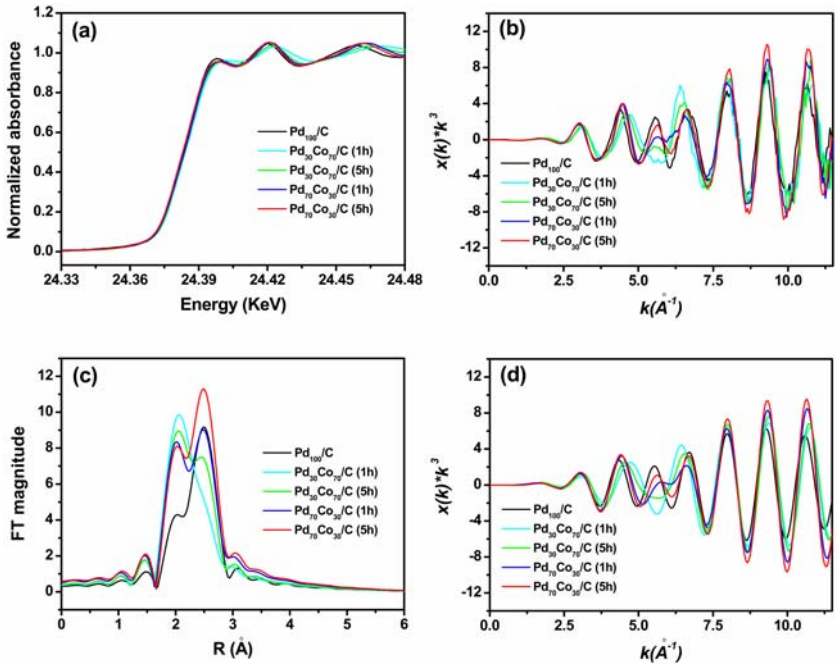

Fig. 3. X-ray Absorption at the Pd K-edge for (a) XANES spectra, (b) experimental data, (c) Fourier transform magnitude of the radial distribution function and (d) k^3- weighted EXAFS spectra.

shows Fourier transform magnitude of the radial distribution function at the Pd K-edge. The processed spectra by using a program IFEFFIT show the simulated geometric information of EXAFS data of PdCo electrocatalysts in Fig. 4(a) and Table 2. Coordination number of Pd-Pd was increased but that of Pd-Co was decreased in PdCo/C with increasing heating time in Fig. 4(b), meaning that that the formation of bimetallic particles with a central core of Co surrounded by an outer Pd-rich layer. In addition, due to the segregation of Pd and Co, the repulsive force was increased in the each of Pd and Co, which is the reason why 1NN of Pd-Pd and Pd-Co in R-range was increased in Fig 4(c). $Pd_{70}Co_{30}$/C electrocatalysts relatively showed higher coordination number of Pd-Pd pair than $Pd_{30}Co_{70}$/C electrocatalysts. Therefore, although $Pd_{30}Co_{70}$/C (1 h) had the structure of Pd and Co alloy, $Pd_{30}Co_{70}$/C (5 h) electrocatalysts changed to the core-shell structure of PdCo alloy as increasing heating time. On the other hand, $Pd_{70}Co_{30}$/C (1 h) electrocatalysts had the core-shell structure of PdCo alloy to begin with and had more increased Pd shell structure of PdCo alloy with increased heating time due to the segregation of Pd and Co. Fig. 4(d) shows the change of Debye-Waller factor, a reduction factor for the intensity of coherent scattering of excited electrons by X-ray absorption by thermal motion or static disorder of atom in lattice. Since the EXAFS measurements were performed in the same room temperature, it is possible to discard the effect of thermal vibration. Hence, the change of Debye-Waller factor in this study is completely due to the static disorder in alloy phase or core-shell structure. The Debye-

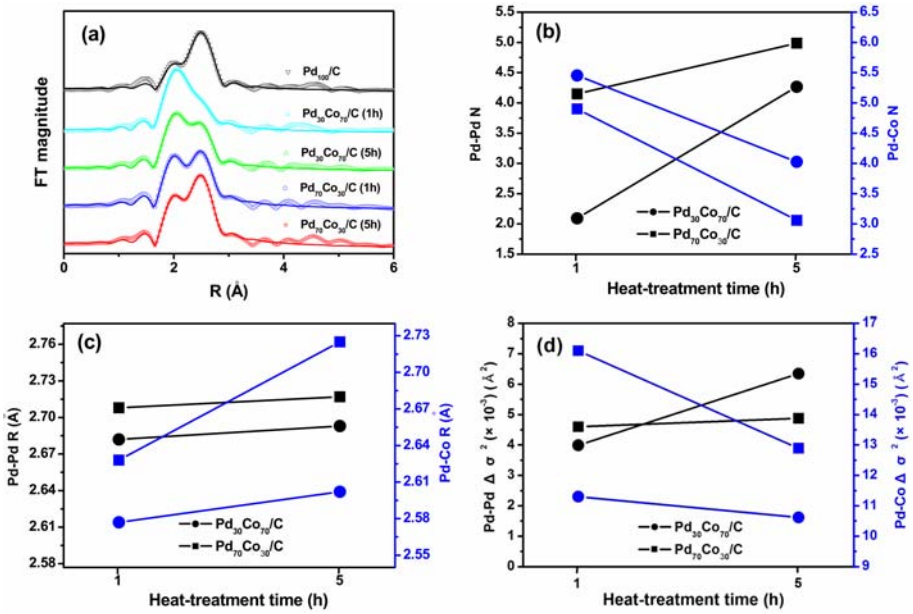

Fig. 4. X-ray Absorption at the Pd K-edge for best-fitting structural parameters of (a) Fourier transform magnitude of the radial distribution function, (b) coordination numbers, (c) bond distance and (d) Debye-Waller factor.

Table 2. Best-fit structural parameters obtained from the analysis of the Pd K-edge EXAFS spectra

catalyst	Pd-Pd pair			Pd-Co pair		
	N	R (Å)	$\Delta\sigma^2$ ($\times10^{-3}$) (Å^2)	N	R (Å)	$\Delta\sigma^2$ ($\times10^{-3}$) (Å^2)
Pd_{100}/C	5.488	2.733	7.674	-	-	-
$Pd_{30}Co_{70}$/C (1 h)	2.093	2.682	3.988	5.454	2.577	11.300
$Pd_{30}Co_{70}$/C (5 h)	4.267	2.693	6.346	4.027	2.602	10.616
$Pd_{70}Co_{30}$/C (1 h)	4.149	2.708	4.596	4.901	2.628	16.100
$Pd_{70}Co_{30}$/C (5 h)	4.988	2.717	4.874	3.059	2.725	12.891

Waller factor for 1NN of Pd-Pd was increased with heat-treatment time, while that for 1NN of Pd-Co was decreased with same condition. This is attributable to the fact that the degree of alloy was decreased (i.e., the increase of phase separation to produce the core-shell structure) with heat-treatment time, so that the possibility of occurrence of static disorder in lattice for Pd-rich phase was increased and on the other hand that for alloy phase was decreased. In addition, 1NN of Pd-Pd in R-range for PdCo/C electrocatalysts was remarkably reduced than Pd_{100}/C electrocatalyst. As a result, a compressive strain was applied on the Pd skin. The core-sell structure substantially modify their electronic structure and catalytic properties because of their interaction of the shell atoms with the core atoms. Therefore, the ε_d could be shifted to a lower-energy position. R.R. Adzic *et al.*[4,33] reported that a combination of the compressive strain effect and ligand effect apparently reduces the adsorption energy of adsorbates by lowering the ε_d of the Pd skin. This is the origin of enhanced ORR kinetics on the PdCo catalyst because it binds oxygen less strongly. In the durability issue of the PdCo/C electrocatalyst, since the durability was lower in the condition of the leaching out of the poorly alloyed Co,[35] the introduction of the core-shell structure of PdCo is the positive factor for the better durability of PdCo alloy electrocatalysts.

The cyclic voltammetry (CV) of Pd_{100}/C and a series of PdCo/C electrocatalysts in N_2-saturated 0.1 M $HClO_4$ electrolyte solutions at a scan rate of 20 mV/s is presented in Fig. 5(a). All of the electrocatalysts clearly exhibited typical features associated with the hydrogen adsorption/desorption and preoxidation/reduction peaks. Pd_{100}/C showed the largest area of the hydrogen adsorption/desorption than PdCo/C electrocatalysts becasue of the smallest particle size of Pd. However, the onset potential for the Pd oxide formation in the positive scan and the oxide reduction in the negative scan were shifted to more positive potential for all of the PdCo/C catalysts as compared to Pd_{100}/C. This observation indicates that the PdCo catalysts-could effectively retard the chemisorption of oxygenated species such as OH_{ad} on the Pd sites at high potential by the change in the Pd electronic structure induced by the addition of Co. This should be beneficial to the oxygen adsorption at low potential with the ORR kinetic enhancement.[3]

The oxygen reduction reaction (ORR) of Pd_{100}/C and a

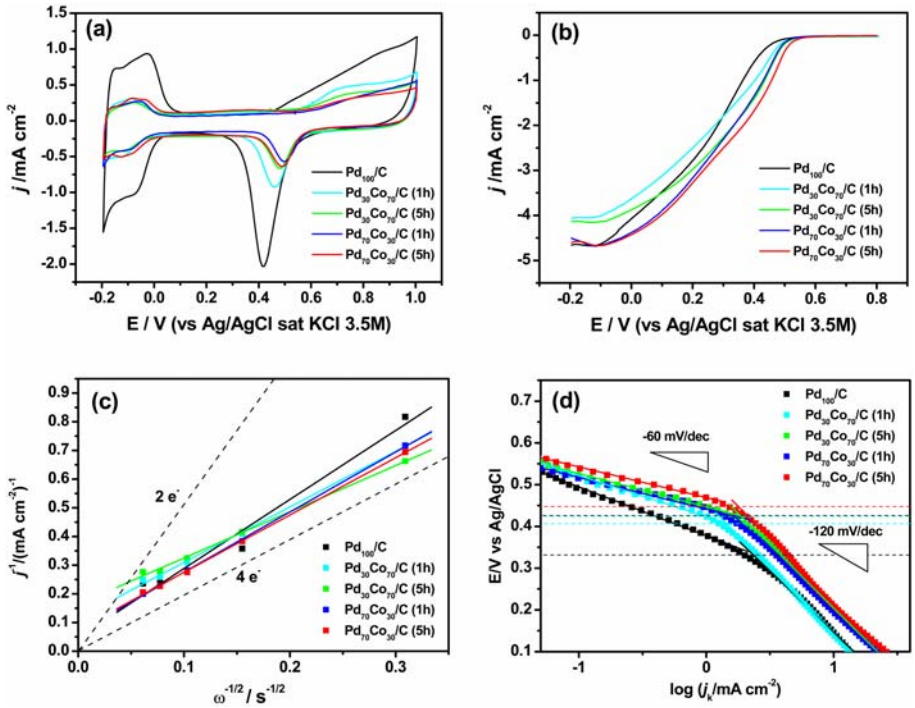

Fig. 5. (a) Cyclic voltammograms of the Pd_{100}/C and Pd_xCo_{100-X} electrocatalysts (b) Compared ORR at the 1600 rpm. (c) Koutecky-Levich plots for ORR at 0.4 V vs Ag/AgCl. (d) Tafel plots for ORR (dashed lines indicate transition potential from low Tafel slope to high Tafel slope)

series of PdCo/C electrocatalysts in O_2-saturated 0.1 M $HClO_4$ electrolyte solutions at a rotating speed of 1600 rpm with a scan rate of 5 mV/s is presented in Fig. 5(b). The onset potential for all of the electrocatalysts was increased in following sequence: Pd_{100}/C < $Pd_{30}Co_{70}$/C(1 h) < $Pd_{30}Co_{70}$/C(5 h) ≤ $Pd_{70}Co_{30}$/C(1 h) < $Pd_{70}Co_{30}$/C(5 h). All of the PdCo/C electrocatalysts had significant enhancement on the onset potential compared to Pd_{100}/C, which shows the PdCo electrocatalysts has better ORR activity than pure Pd electrocatalyst due to the ligand effect.[4] In addition, the onset potentials of PdCo/C electrocatalysts were increased as increasing the heat-treatment time, meaning that the introduction of the core-shell structure of PdCo had a positive effect on the ORR activity as shown in XAS study. In particular, $Pd_{70}Co_{30}$/C(5 h) showed the highest onset potential with the best core-shell structure of PdCo revealed in EXAFS fitting, implying that that $Pd_{70}Co_{30}$/C(5 h) electrocatalyst has the best fine structure for the ORR activity.

The measured electrode current densities at constant potentials were applied to the Koutecky-Levich plot[36] to indicate first-order kinetics with respect to molecular oxygen with representing the inverse current densities (j^{-1}) as a function of the inverse of the square root of the rotation rate ($\omega^{-1/2}$) in Fig. 5(c). From the Koutecky-Levich equation

$$\frac{1}{j} = \frac{1}{j_k} + \frac{1}{j_d} = \frac{1}{j_k} + \frac{1}{B\omega^{1/2}} \quad (1)$$

in which

$$B = \frac{0.62nFACo_2Do_2^{2/3}}{\eta^{1/6}} \quad (2)$$

where j is the experimentally obtained current, j_k is the kinetic current, j_d is the diffusion limiting current, n is the number of electrons transferred, F is Faraday's constant (F = 96485.3399 C/mol), A is the electrode's geometric area (A = 0.19625 cm^2), C_{O2} is the O_2 concentration in the electrolyte (C_{O2} = 1.26 × 10^{-3} mol/L), D_{O2} is the diffusion coefficient of O_2 in the $HClO_4$ solution (D_{O2} = 1.93 × 10^{-5} cm^2/s), and η is the viscosity of the electrolyte (η = 1.009 × 10^{-2} cm^2/s).[37] The slope of the inset plot (j^{-1} vs. $\omega^{-1/2}$) is 1/B. The calculated values of B are 0.0915 mA $s^{-1/2}$ on PdCo/C electrocatalysts, which means that the calculated number of transferred electrons were found to be 3.99 electron. However, Pd_{100}/C shows 0.0816 mA $s^{-1/2}$ of B value, which is 3.56 electron. We can therefore conclude that the core-shell structure of PdCo/C electrocatalysts can have 4 electron charge of the ORR activity.

The Tafel plot of the kinetic current, $j_k = j_d j/(j_d - j)$, of all of the electrocatalysts is shown in Fig. 5(d). Two Tafel slope regions, –60 mV/dec and –120 mV/dec, were observed for PdCo/C electrocatalysts. The transition of the Tafel slope from the low Tafel slope to the high Tafel slope on PdCo is related to their oxides, which were formed from the reaction of H_2O with Pd.[38] The transition potential, dashed lines in Fig. 5(d), from the low Tafel slope to the high Tafel slope for all of the electrocatalysts were increased in following sequence: Pd_{100}/C < $Pd_{30}Co_{70}$/C (1 h) < $Pd_{30}Co_{70}$/C(5 h) ≤ $Pd_{70}Co_{30}$/C(1 h) < $Pd_{70}Co_{30}$/C (5 h). Among them, $Pd_{30}Co_{70}$/C (5 h) and $Pd_{70}Co_{30}$/C (1 h) showed the similar transition potential. This result indicates that depending on the structure of PdCo, PdCo electrocatalysts can have a competitive ORR activity despite the smaller ratio of Pd. In particular, $Pd_{70}Co_{30}$/C (5 h) was 116 mV higher than Pd_{100}/C. It is consequently considered that the ORR activity of Pd based electrocatalyst can be dramatically enhanced by forming the core-shell structure of PdCo/C electrocatalysts. In addition, this improvement is based from the down shift of the d-band center by lowering Pd-O bond strength, which has led to higher activity for the ORR. As shown above, these results are highly in accordance with XAS data. Consequently, we have found that the introduction of the core-shell structure of PdCo is the key factor to enhance the ORR activity by increasing the heating time and it was successfuly studied by XAS technique.

4. Conclusions

We have investigated on the fine structure effect of PdCo electrocatalyst on oxygen reduction reaction activity with different heat-treatment time. There was not the significant increase in PdCo particle size with increasing heat-treatment time in TEM image. In XRD patterns, the low angle shift of Pd(111) peak was shown for PdCo/C samples with increasing heat-treatment time from 1 h to 5 h, meaning that the lattice constant was decreased by alloying with Co having smaller atomic radius. The XAS technique was also used to extract the structural parameters required for understanding the atomic distribution and alloying extent by revealing the corresponding simulated structure. It was revealed that $Pd_{70}Co_{30}$/C (1 h) electrocatalysts had the core-shell structure of PdCo alloy and has more increased Pd-rich phase on the surface of PdCo alloy with increased heat treatment time due to the segregation of Pd and Co. In addition, although $Pd_{30}Co_{70}$/C (1 h) has the random structure of Pd and Co alloy, $Pd_{30}C_{70}$/C

electrocatalysts has changed into the core-shell structure of PdCo alloy with increasing heat treatment time. Furthermore, since the Pd interatomic distance in the PdCo alloy was much smaller than that of pure Pd particles, it was identified that the compressive strain was applied on the Pd-skin. The ε_d could be therefore shifted to a lower-energy position from the Fermi level by introducing the core-shell structure of PdCo electrocatalysts. Hence, we can conclude that the core shell structure resulted from the enough heat treatment is very advantageous form for the oxygen reduction reaction for Pd-based alloy electrocatalysts.

Acknowledgment

This work was supported for two years by Pusan National University Research Grant.

Reference

1. S. Mukerjee, S. Srinivasan, M.P. Soriaga, and J. McBreen, *J.Electrochem. Soc.*, **142**, 1409 (1995).
2. S.F. Parker, C.D. Frost, M. Telling, P. Albers, M. Lopez, and K. Seitz, *Catal. Today*, **114**, 418 (2006).
3. F.J. Lai, L.S. Sarma, H.L. Chou, D.G. Liu, C.A. Hsieh, J.F. Lee, and B.J. Hwang, *J. Phys. Chem. C*, **113**, 12674 (2009).
4. M.H. Shao, T. Huang, P. Liu, J. Zhang, K. Sasaki, M.B. Vukmirovic, and R.R. Adzic, *Langmuir*, **22**, 10409 (2006).
5. M.H. Shao, K. Sasaki, and R.R. Adzic, *J. Am. Chem. Soc.*, **128**, 3526 (2006).
6. V. Raghuveer, P.J. Ferreira, and A. Manthiram, *Electrochem. Commun.*, **8**, 807 (2006).
7. V. Raghuveer, A. Manthiram, and A. J. Bard, *J. Phys. Chem. B*, **109**, 22909 (2005).
8. J.L. Fernandez, V. Raghuveer, A. Manthiram, and A.J. Bard, *J. Am. Chem. Soc.*, **127**, 13100 (2005).
9. A. Ishihara, Y. Shibata, S. Mitsushima, and K. Ota, *J. Electrochem. Soc.*, **155**, B400 (2008).
10. R.R. Adzic, J. Zhang, K. Sasaki, M.B. Vukmirovic, M. Shao, J.X. Wang, A.U. Nilekar, M. Mavrikakis, J.A. Valerio, and F. Uribe, *Top. Catal.*, **46**, 249 (2007).
11. H. Liu and A. Manthiram, *Energy Environ. Sci.*, **2**, 124 (2009).
12. H. Liu and A. Manthiram, *Electrochem. Commun.*, **10**, 740 (2008).
13. L. Zhang, K. Lee, and J. Zhang, *Electrochim. Acta*, **52**, 3088 (2007).
14. G. Bozzolo, R.D. Noebe, J. Khalil, and J. Morse, *Appl. Surf. Sci.*, **219**, 149 (2003).
15. J.L. Rousset, J.C. Bertolini, and P. Miegge, *Phys. Rev. B*, **53**, 4947 (1996).
16. B. Hammer, J.K. Nørskov, C.G. Bruce, and K. Helmut, *Advances in Catalysis*, Academic Press, California (2000).
17. J.R. Kitchin, J.K. Nørskov, M.A. Barteau, and J.G. Chen, *J. Chem. Phys.*, **120**, 10240 (2004).
18. B. Mierzwa, *J. Alloy. Compd.*, **362**, 178 (2004).
19. S. Mukerjee and J. McBreen, *J. Electroanal. Chem.*, **448**, 163 (1998).
20. S. Mukerjee, S. Srinivasan, M.P. Soriaga, and J. McBreen, *J. Electrochem. Soc.*, **142**, 1409 (1995).
21. F.B. Noronha, M. Schmal, B. Moraweck, P. Delichere, M. Brun, F. Villain, and R. Frety, *J. Phys. Chem.*, **104**, 5478 (2000).
22. J. Greeley, J.K. Nørskov, and M. Mavrikakis, *Annu. Rev. Phys. Chem.*, **53**, 319 (2002).
23. B. Hammer and J.K. Nørskov, *Surf. Sci.*, **343**, 211 (1995).
24. M. Newville, *J. Synchrotron Radiat.*, **8**, 322 (2001).
25. B. Ravel, *J. Synchrotron Radiat.*, **8**, 314 (2001).
26. B. Ravel and M. Newville, *J. Synchrotron Radiat.*, **12**, 537 (2005).
27. M. Newville, *J. Synchrotron Radiat.*, **8**, 96 (2001).
28. M. Newville, P. Līviņš, Y. Yacoby, J.J. Rehr, and E.A. Stern, *Physical Review B*, **47**, 14126 (1993).
29. J.J. Rehr and R.C. Albers, *Rev. Mod. Phys.*, **72**, 621 (2000).
30. S.P. Jiang, Z. Liu, H.L. Tang, and M. Pan, *Electrochim. Acta*, **51**, 5721 (2006).
31. J. Zhang, Y. Mo, M.B. Vukmirovic, R. Klie, K. Sasaki, and R.R. Adzic, *J. Phys. Chem. B*, **108**, 10955 (2004).
32. F.H.B. Lima, J. Zhang, M.H. Shao, K. Sasaki, M.B. Vukmirovic, E.A. Ticianelli, and R.R. Adzic, *J. Phys. Chemistry B*, **111**, 404 (2007).
33. F.H.B. Lima, J. Zhang, M.H. Shao, K. Sasaki, M.B. Vukmirovic, E.A. Ticianelli, and R.R. Adzic, *J. Solid State Electr.*, **12**, 399 (2008).
34. A.U. Nilekar, Y. Xu, J.L. Zhang, M.B. Vukmirovic, K. Sasaki, R.R. Adzic, and M. Mavrikakis, *Top. Catal.*, **46**, 276 (2007).
35. H. Liu, W. Li, and A. Manthiram, *Appl. Catal. B-Environ.*, **90**, 184 (2009).
36. M.H. Shao, P. Liu, and R.R. Adzic, *J. Am. Chem. Soc.*, **128**, 7408 (2006).
37. D.-S. Kim, E.F.A. Zeid, and Y.-T. Kim, *Electrochim. Acta*, **55**, 3628.
38. K. Lee, O. Savadogo, A. Ishihara, S. Mitsushima, N. Kamiya, and K.-i. Ota, *J. Electrochem. Soc.*, **153**, A20 (2006).